arXiv:astro-ph/0410162v1 6 Oct 2004

An X–ray View of WLRGs/LINERs

Alexander S. Rinn, Rita M. Sambruna, and Mario Gliozzi

George Mason University, Dept. of Physics and Astronomy, MS 3F3, 4400 University Drive, Fairfax, VA 22030

ABSTRACT

We present X–ray observations of nine Weak-Line Radio Galaxies (WLRGs), optically classified as confirmed or possible Low Ionization Nuclear Emission–line Regions (LINERs). The data were taken from the *Chandra*, *XMM–Newton*, and *BeppoSAX* archives. The *Chandra* images typically show complex X-ray morphologies, with hard (2–10 keV) point sources embedded in diffuse soft (0.3–2.0 keV) emission in all cases except 1246–41 (NGC 4696), where only diffuse emission is detected on the scale of the cluster, and 0334–01 (3C 15), where only a point source is detected. The nuclear X–ray spectra are well fitted at hard energies by an absorbed power law, with a wide range of photon indices, $\Gamma = 1.5-2.7$. Excess absorption over the Galactic value is detected in 6/9 sources, with column densities $N_H \approx 10^{21-22}$ cm^{-2}. A thermal component is required at softer energies, in agreement with the results of the spatial analysis. We find that there is no correlation between the core X–ray luminosity and the radio core dominance parameter, suggesting that the bulk of the core X-ray emission is not beamed, but rather is isotropic and thus likely related to the accretion flow. In an attempt to constrain the nature of the accretion flow, we calculate the ratios of bolometric to Eddington luminosities L_{bol}/L_{Edd}, and the radiative efficiency η based on the Bondi accretion rates. We find that $L_{bol}/L_{Edd} \sim 10^{-4} - 10^{-6}$ and $\eta \sim 10^{-2} - 10^{-6}$ for all the objects in our sample, suggesting radiatively inefficient accretion flows.

Subject headings: galaxies: active—galaxies: nuclei—X-rays: galaxies

1. Introduction

The recent discovery of *HST* and ground–based observations that most nearby galaxies harbor supermassive black holes (Kormendy & Richstone 1995; Richstone et al. 1998), along with independent evidence that weak nuclear activity is very common in both spiral

and elliptical galaxies (Heckman 1980; Sadler et al. 1989; Tadhunter et al. 1998), affirms the fundamental link between "normal" and active galaxies. According to the Palomar survey (Ho et al. 1997), over 40% of nearby galaxies ($z \approx 0$) contain low–power Active Galactic Nuclei (AGN), with typical bolometric luminosities lower than 10^{44} erg s^{-1}. Most of these, based on their low–ionization spectra, are classified as Low Ionization Nuclear Emission–line Regions (LINERs), or transition objects. Since accreting supermassive black holes are widely held to be responsible for the nuclear activity in AGN, one naturally wonders why such intense nuclear activity is limited to a minority of galaxies. A possible explanation is that obscuring material along the line of sight conceals the nuclear activity. Alternatively, there could be inefficient accretion onto the black hole due either to a low accretion rate (the AGN–starved scenario), or to some kind of radiatively–inefficient accretion flow (RIAF; see e.g. Quataert 2003). Weak AGN, such as those hosted by nearby low–power radio galaxies in giant ellipticals, may represent the link between powerful AGN and "normal" galaxies.

One class of objects that may represent this link are Weak–Line Radio Galaxies (WLRGs; Tadhunter et al. 1998), which are classified by [O III]λ5007 luminosities more than 10 times lower than those of the general population at similar redshifts. The weakness of the [O III]λ5007 emission line in WLRGs raises the possibility that these objects may be related to LINERs; indeed, there is evidence that WLRGs and LINERs are intimately related (Lewis et al. 2003). If all LINERs can be regarded as true AGN, then they would constitute approximately 75% of all AGN (Ho et al. 1997). Put in this light, WLRGs/LINERs could prove essential to understanding the link between "normal" and active galaxies.

X–rays provide us with a powerful tool by which we can achieve progress in our understanding of the nature of accretion in low-power AGN, because they originate in the innermost, hottest parts of the accretion flow. In addition, soft X–rays map the distribution of the circumnuclear gas around the nuclei, allowing us to quantify the fuel reservoir on the nucleus.

In Section 2 we describe our sample of WLRGs/LINERs. In Section 3 we describe the observations and data reduction. Section 4 contains the results of the spatial analysis based on *Chandra* observations (4.1), and the results of the temporal and spectral analysis (Sections 4.2 and 4.3, respectively), both of which are based on *Chandra*, *XMM–Newton*, and *BeppoSAX* observations. In Section 5 we discuss the obscuration and nature of accretion in WLRGs/LINERs, as well as some comparisons with the results of previous work. Finally, in Section 6 we summarize our results. Throughout the paper we use a Friedman cosmology with $H_0 = 75$ km s^{-1} and $q_0 = 0.5$.

2. The Sample

Our sample consists of 9 out of the 24 WLRGs that comprise the Lewis, Eracleous, & Sambruna (2003) sample. That sample was selected in order to investigate the relationship between WLRGs and LINERs. Our 9 sources were selected based on two criteria: first, that Lewis et al. classified the source as a LINER, as a possible–LINER, or that there were conflicting classifications; second, that there existed X–ray observations for the sources made by either *Chandra*, *XMM–Newton*, or *BeppoSAX*.

Table 1 lists some characteristics of the sources in our sample. It should be noted that all of the sources have redshifts z <0.1. The black hole masses were calculated using the relationship $M_{BH} = 1.3 \times 10^8 (\sigma/200\text{km s}^{-1})^{4.58}$ (Ferrarese 2000; Merloni et al. 2003) and using velocity dispersions from the on line catalog HyperLeda (http://foehn.univ-lyon1.fr/hypercat/-search.html), unless otherwise specified in the table. These calculations were consistent with those found in the literature. Also, there is only one source that is classified as an FRII (1637–77); the rest of the sources are classified as either FRIs or transition objects FRI/II. Finally, we list how Lewis et al. (2003) classified the sources: 6 of the sources are confirmed LINERs, 2 are possible LINERs, and 1 is conflicting.

3. Observations and Data Reduction

Table 2 summarizes the X–ray observations of the sources comprising our sample. We used 7 *Chandra* observations, 4 *XMM–Newton* observations, and 1 *BeppoSAX* observation.

3.1. *Chandra*

All of the *Chandra* observations were made using the ACIS–S detector. Pile–up was not a problem in any of the observations. The data reduction was performed with CIAO v. 2.3 and CALDB v. 2.18. The data were reprocessed with `acis_process_events` and screened to exclude periods of background flaring. In order to take into account the continuous degradation of the ACIS quantum efficiency (QE) due to molecular contamination of the optical blocking filters, we applied `ACISABS` to the ancillary response function (ARF) file.

The spectra were rebinned (with the exception of 1251–12) such that each spectral bin contained at least 20 counts in order to apply χ^2 minimization, and fitted using the XSPEC v. 11.2 software package (Arnaud 1996). Due to the very low number of counts, we did not rebin the spectrum of 1251–12, and instead of the χ^2 statistics, we used the C–statistics

when fitting the spectrum. The quoted errors on the derived best–fit model parameters correspond to a 90% confidence level. The latest publicly available responses were used. The same procedure was applied to the *XMM–Newton* and *BeppoSAX* spectral analysis.

3.2. *XMM–Newton*

The *XMM–Newton* analysis was based on the EPIC pn data, since they have the highest signal–to–noise ratio among the EPIC cameras. For 0915–11 and 1637–77 the EPIC pn operated in full-frame extended mode with a thin filter. For 1216+06 and 1246–41 the EPIC pn operated in full–frame mode with a thin filter. The recorded events were reprocessed and screened with the latest available release of the *XMM–Newton* Science Analysis Software (SAS 5.4) to remove known hot pixels and other data flagged as bad—only data with `FLAG=0` were used. We investigated the full-field light curves to detect periods of background flaring; any such events were screened. In 0915–11, 1216+06, and 1637–77 background data were extracted from a source–free circular region on the same chip containing the source. In 1246–41 background data were extracted in an annular region centered about the nuclear extraction region; this was done in an attempt to take into account the cluster in which this source lies. There are no signs of pile-up in any of the sources.

3.3. *BeppoSAX*

BeppoSAX observed 0305+03 (3C 40) with the Narrow Field Instruments, LECS (0.1–4.5 keV) and MECS (1.3–10.0 keV) on 1997 January 07, with effective exposures of 8.7 ks and 19.4 ks respectively. The LECS and MECS are both imaging instruments. The observations were performed with 2 active MECS units. Standard data reduction techniques were employed, following the prescription given by Fiore et al. (1999). LECS and MECS spectra and light curves were extracted from regions with radii of 8' and 4' respectively, in order to maximize the accumulated counts at both low and high energies. Background spectra were extracted from high Galactic latitude "blank" fields. The background subtracted count rates are $(3.7 \pm 0.3) \times 10^{-2}$ cnts s^{-1} for the LECS in the 0.1–4.5 keV band, and $(3.5 \pm 0.1) \times 10^{-2}$ cnts s^{-1} for the MECS in the 2–10 keV energy band.

4. Results

4.1. Spatial Analysis

Chandra's subarcsecond spatial resolution provides us with the opportunity to disentangle the different X–ray components in a given source. In particular, the detection of a hard X–ray nuclear point source lends support to the claim that a source houses an AGN. Whatever the results of the spatial analysis are, they help one to better constrain and interpret the spectral data associated with the source.

For each of the objects in our sample observed by *Chandra* (except 1216+06, for which a more detailed spatial analysis is given in Gliozzi et al. 2003), Fig. 1 shows the adaptively smoothed images in the energy band 0.3–10 keV with hard X–ray contours superimposed (2–10 keV); also shown are the surface brightness profiles. The images were smoothed using `fadapt` from the `ftools` software package. To produce the surface brightness profiles, we first used the source energy spectrum to derive the appropriate Point Spread Function (PSF) with ChaRT (http://cxc.harvard.edu/soft/ChaRT/cgi-bin/www-saosac.cgi). We then fit the ChaRT PSF in order to find an analytic description of it. Next we fit the total surface brightness profile with both the analytic PSF and either one or two β–models (e.g., Cavaliere & Fusco-Femiano 1976) in order to describe the extended emission. Finally, we used an F–test to assess the significance of the PSF by comparing the PSF plus β–model to a β–model alone.

The results of the spatial analysis are summarized in Table 3. All the objects, except 1246–41, required a PSF at high significance level. We found that only 0034–01 required no β–model; it was fit well by the PSF plus the background. The object 0915–11 was fit well by a PSF plus β–model out to $\approx$25 arcseconds. Past $\approx$25 arcseconds the source appears to require another β–model, but we could not get good statistics on a second β–model—perhaps because the field of view was not large enough. We found that 1246–41 does not require a PSF, and while it too appears to require an additional β–model past $\approx$25 arcseconds, we could not get good statistics on a second β–model. For 1333–33 it was required to fix the value for the core radius in order to arrive at physically meaningful results—several different values were tried, with the quoted value yielding the best fit.

4.2. Timing Analysis

We produced background subtracted light curves for each of the objects in our sample. For 1216+06 we refer to the detailed study by Gliozzi, Sambruna, & Brandt (2003). We

chose to produce light curves based on *XMM–Newton* data when possible, but when only *Chandra* or *BeppoSAX* data were available, those data were used. According to a χ^2 test for constancy, we found there to be no statistically significant nuclear variability in any of the objects on the time scales probed by our observations, $\sim$ few hours. This is likely due to (1) the intrinsic weakness of the sources, which translates into a low count–rate especially for *Chandra* and *BeppoSAX* observations, and (2) the short exposures.

4.3. Spectral Analysis

Previous X–ray spectral studies of low power radio galaxies suggest that at least two components are required to fit a spectrum: one, a thermal component associated with the extended emission; two, a power–law component associated with the unresolved nuclear point source (Worrall & Birkinshaw 1994). This is consistent with the results of our spatial analysis, in which four out of the six sources required a point–like source in diffuse emission. With these considerations in mind we began our spectral modeling with a power law, which dominates at hard energies, and a soft component modeled as emission from a collisionally–ionized plasma (`apec` in `XSPEC`; Smith et al. 2001). All of the spectral models also assume a column density fixed to the Galactic level appropriate to the source (Dickey & Lockman 1990). Additional components, such as intrinsic absorption, covering fraction, or additional thermal components, were added to the model when the data required them.

The results of the spectral analysis are summarized in Table 4. When a source was observed with both *XMM–Newton* and *Chandra* we quote the spectral model derived from the *XMM–Newton* data, since it was more statistically sound. Seven out of the nine objects require a power law with Γ between ~ 1.5 and ~ 2.7, with the average value being ~ 1.9. The extremely flat value of Γ for 1251–12 might be related to the poor photon statistics. Six out of the nine objects required at least one thermal component. The temperatures show a bimodal distribution around 0.6 keV and > 1.5 keV, which probably reflects the different environments—poor and rich clusters respectively. Five out of the nine objects required intrinsic absorption with values ranging from $\sim 10^{21}$ to $\sim 10^{23}$ cm^{-2}, with the average value being $\sim 4 \times 10^{23}$. We tried to add a Fe Kα line at 6.4 keV, but this was not statistically required for any of the objects except 1216+06 (see Sambruna et al. 2003).

The spectral results are in good agreement with the findings of the spatial analysis. The surface brightness profile of 0034–01 was found to not require a β–model, indicating that little to no extended emission is present; indeed, we see that no thermal component is required to fit the object's spectrum. We also found that the surface brightness profile of 1246–41 did not require a PSF, indicating a heavily absorbed and/or very weak point source;

this too conforms to the spectral results, in that no power law was required to fit the object's spectrum.

5. Discussion

This paper seeks to shed light on the role of WLRGs/LINERs in the context of uncovering the relationship between "normal" galaxies and powerful AGN. The results of the X–ray analysis allow us to address several important questions towards this end: (1) What is the role of obscuration in WLRGs/LINERs? (2) What is the nature of accretion in such objects? (3) How do the X–ray properties of WLRGs/LINERs compare to those of other classes of radio galaxies?

5.1. The role of obscuration

According to the unified model of AGN (e.g., Urry & Padovani 1995), the central regions of AGN appear to contain a molecular torus that prevents the penetration of radiation from the nucleus along certain lines of sight. This can cause intrinsically similar AGN to look remarkably different from different viewing angles. Recently, however, the presence of an obscuring torus in low–power radio galaxies, specifically FRIs, has been called into question (Chiaberge et al. 1999; Capetti et al. 2002, henceforth C99C02), based on *HST* observations of the 3C and B2 catalogs. Since our sample is composed of low–power radio galaxies, and because our analysis is focused on the X–rays, we are in a position to contribute to this debate. X–rays, due to their high penetrating power, are the ideal means by which the presence of an obscuring torus can be investigated.

The results of our spectral analysis show that 4 of the 9 objects in our sample require an absorption component on the order of 10^{22} cm^{-2}, which qualifies as significant absorption. Out of those 4 objects, 3 are confirmed LINERs, while 1 is classified as conflicting. In addition to these 4 objects there are 2 others that, while not heavily absorbed, require an absorption component on the order of 10^{21} cm^{-2}; one of these additional objects is a confirmed LINER, the other is a possible LINER. Thus, 6 of 9 objects in our sample show signs of absorption, which suggests that some low–power radio galaxies may indeed house obscuring tori. Moreover, all 6 of these absorbed objects are classified as FRIs or FRI/FRIIs , which is in contrast to the hypothesis that low–power radio galaxies, specifically FRIs, lack a molecular torus (C99C02). The apparently surprising result that the only FRII in our sample (1637–77) is not absorbed may be explained if the object can be classified as

a Low Excitation Galaxy (LEG); Chiaberge, Capetti, & Celotti (2002) explain that, while LEGs may be classified morphologically as FRIIs, their radio to optical nuclear properties are indistinguishable from FRIs. The [O II]/[O III] ratio for 1637–77 places it right on the border of the LEG classification, but if 1637–77 can be classified as an LEG, we should expect it to be unabsorbed.

In order to address the apparent discrepancy between the optical/UV and the X–ray absorption properties, one must keep in mind that the inner regions of the accretion flow ($\sim 10 - 50$ R_G), where most of the radiation is supposed to originate, is inaccessible to any observatory. Even though the angular resolution of *HST* (~ 0.1 arcseconds) is much better than *Chandra* (~ 1.0 arcseconds) and *XMM–Newton* (~ 10 arcseconds), the region probed by *HST* is not closer to the black hole than the X–ray satellites. Indeed, assuming a typical black hole mass of 5×10^8 $M_\odot$ at a distance of 40 Mpc (corresponding to $z \sim 0.01$), the inner 50 R_G subtends a region of angular size $\sim 10^{-4}$ arcseconds, which is three orders of magnitude smaller than the spatial resolution of *HST*. This indicates that the unresolved X–ray and optical sources simply reflect the PSF of the respective instrument rather than the physical size of the emitting regions.

In light of these considerations, it is entirely possible that the X–ray emission is produced in a region closer to the black hole than that of the optical/UV emitting region. Indeed, theoretical arguments predict that the location of the X–ray emitting region is closer to the black hole in both accretion and jet models. This hypothesis is supported by the difference in absorption properties found in the optical/UV and the X-rays, if it is assumed that two distinct media are responsible for the absorption (Weingarter & Murray 2002; Sambruna et al. 2003; Lewis et al. 2003). In this theory the optical/UV absorber is a dusty medium lying farther away from the nucleus than the X–ray absorber, which is a neutral or ionized gas largely free of dust. Further support for the hypothesis that the X–rays are produced in a region interior to the optical/UV emitting region comes from the recent work of Donato, Sambruna, & Gliozzi (2004). Those authors find that a substantial fraction of the compact cores detected in the optical (Chiaberge et al. 1999), do not have an unresolved X–ray counterpart, which suggests a different origin and/or nature for optical/UV and X-ray radiation. Additionally, Donato et al. show that neither X–ray obscuration nor the detection of unresolved X–ray cores is related to the presence of dust lanes, which are responsible for the optical absorption. Finally, we note that there is no discrepancy between this paper and Donato et al. (2004) concerning obscuration; in that paper all the FRIs except the LINER 1216+06 (NGC 4261) show negligible absorption ($N_H < 10^{21}$ cm^{-2}). This suggests that the absorption mechanisms in WLRGs/LINERs may be different than those in other low–luminosity radio galaxies.

5.2. The nature of accretion

The origin of X–rays in radio galaxies is a topic of considerable debate. Specifically the question is: Do X–rays have their origin in the process of accretion or at the unresolved base of the jet? The correlation between the radio and X–ray core luminosities in low and high luminosity radio galaxies (e.g., Fabbiano et al. 1984; Canosa et al. 1999; Worrall & Birkinshaw 1994; Hardcastle et al. 1998) has often been used as an argument in favor of a common origin at the base of the jet. However, this correlation has recently been shown by Merloni, Sebastian, & Di Mateo (2003) to derive from a more general correlation involving both the X–ray luminosity and the black hole mass—the so–called "fundamental plane"—in which the radio is related to the jet, and the X–rays are related to inefficient accretion onto the black hole.

This idea is supported by the detailed study of 1216+06 (NGC 4261) by Gliozzi et al. (2003)—their argument is summarized by three main points: (1) they found there to be a high Bondi accretion rate along with a low AGN luminosity, suggesting the presence of a radiatively inefficient accretion flow; (2) they observed an Fe line at ≈ 7 keV of nuclear origin; (3) they studied the temporal and spectral variability, and combined this with independent information on jet energetics, which lead them to conclude that the bulk of the X–ray emission originates from a radiatively inefficient accretion flow, with negligible jet contribution. Based on the similarity between 1216+06 and the other objects in our sample, we explored the possibility that the X–rays for all the objects in our sample are related to accretion and not the base of the jet.

One way to explore the origin of nuclear emission is via the correlation (or lack thereof) with the radio core dominance ($R = L_{core}/L_{lobe}$)—this has been done in the optical by Kharb & Shastri (2004). By demonstrating a strong correlation between optical point–like emission and radio core dominance, Kharb & Shastri found the optical emission to be strongly beamed, and thus produced by the jet, confirming the results of Chiaberge, Capetti, & Celotti (1999). We adopted this approach for our X–ray sample (see Fig. 2, Table 6), but found there to be no correlation between the core X–ray emission and the radio core dominance, indicating that the emission is not beamed, but rather is isotropic and thus likely to be related to accretion. On the other hand, there is some indication that in non–LINER FRIs at least a fraction of the X–ray emission is beamed, and thus related to the base of the jet (Donato et al. 2004).

Many of the objects in our sample require a powerlaw component for their spectral fit, but the powerlaw components (ranging from $\Gamma \sim 1.5$ to ~ 2.1, excluding the *BeppoSAX* observation with $\Gamma \sim 2.7$) can be a good representation for both jet dominated and accretion dominated emission. The lack of a strong Fe Kα line suggests the lack of a standard accretion disk; however, both the radiatively inefficient accretion and the jet scenario can account for

this result. And while temporal analysis can yield insights into the nature of accretion, our results yield no such clues.

More insightful information comes from the calculations of the bolometric and Eddington luminosities. We used estimates of the black hole masses based on stellar velocity dispersions to calculate $L_{\rm Edd}$, and the relationship $0.1L_{\rm bol} = L_{\rm X}$ in order to calculate $L_{\rm bol}$. For Seyfert–like objects, which are thought to have a standard thin–disk, the ratio of $L_{\rm bol}$ to $L_{\rm Edd}$ is $\sim 10 - 20\%$; an Eddington ratio much less than 10% could signify inefficient accretion. Some accretion properties are listed in Table 5. In our sample we find that the majority of sources have values of $L_{\rm bol}/L_{\rm Edd}$ between 10^{-4} and 10^{-7}. Even the *XMM–Newton* observation of 0915–11, with its high X–ray luminosity, has $L_{\rm bol}/L_{\rm Edd} \sim 10^{-3}$. This is a model–independent indication of Radiatively Inefficient Accretion Flow (RIAF). Using the results of our spatial analysis, specifically the gas density profile obtained by the de–projection of the surface brightness profile, we calculated $\dot{\rm M}_{\rm Bondi}$, which serves as a rough estimate of accretion onto the black hole. With $\dot{M}_{\rm Bondi}$ and $L_{\rm bol}$ we can use the formula $L_{\rm bol} = \eta \dot{M}_{\rm Bondi} c^2$ to make an estimate of the radiative efficiency of accretion η. We find values on the order of $10^{-5} - 10^{-6}$, except for the object 0915–11, which using the *Chandra* observation yields $\eta = 0.01$, and using the *XMM–Newton* observation yields $\eta = 0.09$. Those objects with $\eta << 0.1$ are very likely to have inefficient accretion, but even 0915–11, based on the *Chandra* observation, is a candidate. However, the *XMM–Newton* observation makes the accretion scenario for 0915–11 ambiguous.

5.3. Comparison with previous results

As mentioned above, Donato et al. (2004) have analyzed a larger sample of FRIs from the B2 and 3C catalogues. Those authors found there to be no absorption of X–rays in FRIs, except in the LINER 1216+06 (NGC 4261), which is consistent with our results. While Donato et al. found that the majority of the X–rays in classical FRIs are related to inefficient accretion onto the black hole, their analysis suggests that at least a fraction of the X–rays are beamed and thus potentially related to the base of the jet. This lends further support to the idea that WLRGs/LINERs form a distinct group compared to classical FRIs.

A more general X–ray analysis of radio–loud AGN was made by Sambruna, Eracleous, & Mushotzky (1999) using *ASCA*. In that paper the authors found there to be correlations for the [O III]λ5007, the 5 GHz lobe, and the 12μm luminosities to the 2–10 keV intrinsic X–ray luminosity. Those correlations demonstrated a slight lobe radio excess in WLRGs. We have updated the plots of Sambruna et al. to include those WLRGs that were not in that paper, and have introduced a plot of the 5 GHz core luminosity and the 2–10 keV intrinsic

X–ray luminosity (see Table 6, and Fig. 3). These updated plots show that the WLRGs do indeed demonstrate a lobe radio excess; moreover, they form a distinct class as compared to the other subclasses of radio–loud AGN. To quantify the degree of linear correlation between the 2–10 keV intrinsic luminosity and the 5 GHz lobe radio power for the WLRGs (and the other correlations that follow), we calculated the linear correlation coefficient r and computed the chance probability $P_c(r; N)$ that a random sample of N uncorrelated pairs of measurements would yield a linear correlation coefficient equal to or greater than $|r|$. We also calculated the Spearman and Kendall parameters, which confirm the $P_c(r; N)$ results. We found the probability of correlation between $L_{\rm lobe}$ and $L_{2-10\ \rm keV}$ for the WLRGs to be $\approx 98\%$, with a least squares fit yielding the relationship $\log L_{\rm lobe} = 0.46\ \log L_{2-10\ \rm keV} + 22.6$ $(0.46 \pm 0.1,\ 22.6 \pm 5)$, represented by the dotted line in Fig. 3. The remaining subclasses of AGN formed a distinct group of their own with a probability of correlation $> 99.9\%$; however, the least squares fit of this group yielded a significantly different relationship: $\log L_{\rm lobe} = 0.84\ \log L_{2-10\ \rm keV} + 5.26$ $(0.84 \pm 0.1,\ 5.26 \pm 6)$, represented by the dashed line in Fig. 3. This lobe excess in the WLRGs raises the possibility that there once was much more intense jet activity in these objects than is shown today.

The plot of the core radio power vs. the intrinsic 2–10 keV luminosity shows that the WLRGs follow the correlation of the other subclasses of radio–loud AGN. The probability of correlation is $> 99.9\%$, and a least squares fit yields the relationship $\log L_{\rm core} = 0.51\ \log L_{2-10\ \rm keV} + 18.56$ $(0.51 \pm 0.08,\ 18.56 \pm 3.3)$.

The plot of the MIR luminosity vs. the intrinsic 2–10 keV luminosity suggests that there may also be an MIR excess. However, the MIR data for WLRGs are largely upper limits, so this suggestion should be taken with caution; also, because there were so many upper limits, we were not able to better constrain the correlation found by Sambruna et al. (1999), thus Fig. 3 plots that previously found relationship: $L_{12\mu\rm m} = 0.83\ \log L_{2-10\ \rm keV} + 8.28$. Finally, we found the probability of correlation between $L_{[\rm O_{III}]}$ and $L_{2-10\ \rm keV}$ to be $> 99\%$, with a least squares fit yielding the relationship $\log L_{[\rm O_{III}]} = 1.2\ \log L_{2-10\ \rm keV} - 10.33$ $(1.2 \pm 0.2,\ -10.33 \pm 7)$, which is consistent within the errors with Sambruna et al. (1999). We notice that the WLRGs tend be have a slight [O III] deficiency; however, due to the small number of data points, we could not get good statistics for a least squares fit of the WLRGs as a distinct class.

6. Summary

This paper shows the results of an X–ray analysis of 9 WLRGs/LINERs—the main findings are summarized as follows:

(1) We found that 6 out of the 9 objects in our sample are absorbed in the X–rays. Four of these 6 objects are absorbed on the order of 10^{22} cm^{-2}, which qualifies as significant absorption. The other 2 objects show slightly lower values of absorption (10^{21} cm^{-2}). These results, combined with those of a larger sample of non–LINER FRIs, for which there is a systematic lack of absorption, suggests that WLRGs/LINERs form a distinct class compared to other low–power radio galaxies.

(2) The X–rays in this sample of WLRGs/LINERs appear to be related to accretion. The object 1216+06 has been carefully studied by Gliozzi et al. (2003) and the X–rays of that object are found to be related to accretion. We found that the rest of the objects in our sample behave like 1216+06, and while we can not rule out that a fraction of the X–rays come from the base of the jet, we performed a model independent test and found that the X–rays in this sample do not appear to be beamed. On the other hand, the recent analysis of a sample of classical FRIs reveals that, while the majority of the X–rays are related to inefficient accretion onto the black hole, a fraction of the X–rays may be beamed and thus likely related to the base of the jet. This lends further support to the idea that WLRGs/LINERs form a distinct class compared to other low–power radio galaxies.

(3) Assuming that all the X-ray emission is related to accretion, our tests concerning the nature of accretion are in favor of it being radiatively inefficient. But even if some of the X–rays do stem from the base of the jet, the argument for radiatively inefficient accretion is only strengthened—the fraction of X–rays related to accretion would be even lower than we assumed them to be, which in turn would yield even low efficiency.

Our results are based on a small sample of WLRGs/LINERs. These results should be confirmed by an analysis of a larger sample, which we plan to undertake in a future paper.

We gratefully acknowledge the financial support provided by Smithsonian grant GO3–4123A (ASR), and NASA LTSA grant NAG5–10708 (RMS, MG). RMS gratefully acknowledges support from an NSF CAREER award and from the Clare Boothe Luce Program of the Henry Luce Foundation.

REFERENCES

Arnaud, K. 1996, in Astronomical Data Analysis Software and Systems V, ed. G. Jacoby, & J. Barnes (San Francisco: ASP), ASP Conf. Ser., 101, 17

Bettoni, D., Falomo, R., Fasano, G., & Govoni, F. 2003, A&A, 399, 869

Canosa, C. M., Worrall, D. M., Hardcastle, M. J., & Birkinshaw, M. 1999, MNRAS, 310, 30

Cavaliere, A., & Fusco-Femiano, R. 1976, A&A, 49, 137

Capetti, A., Celotti, A., & Chiaberge, M., et al. 2002, A&A, 383, 104

Chiaberge, M., Capetti, A., & Celotti, A. 1999, A&A, 349, 77

Chiaberge, M., Capetti, A., & Celotti, A. 2002, A&A, 394, 791

Dickey, J. M., & Lockman, F. J. 1990, ARA&A, 28, 215

Di Matteo, T., Quataert, E., Allen, S. W., Narayan, R., & Fabian, A. C. 2000, MNRAS, 311, 507

Donato, D., Sambruna, R. M., & Gliozzi, M. 2004, ApJ in press, [astro-ph/0408451]

Fabbiano, G., Miller, L., Trinchieri, G., Longair, M., & Elvis, M. 1984, ApJ, 277, 115

Fanaroff, B. L. & Riley, J. M. 1974, MNRAS, 167, 31P

Ferrarese, L., Ford, H. C., & Jaffe, W. 1996, ApJ, 470, 444

Ferrarese, L. 2000, "Current High Energy Emission around Black Holes", ed. C.–H. Lee (Singapore: World Scientific),[astro-ph/0203047]

Fiore, F., Guainazzi, M., & Grandi, P. 1999, Handbook for BeppoSAX NFI spectral analysis

Franceschini, A., Vercellone, S., & Fabian, A. C. 1998, MNRAS, 297, 817

Gliozzi, M., Sambruna, R.M., Brandt, W.N 2003, A&A, 408, 949

Golombek, D., Miley, G. K., & Neugebauer, G. 1988, AJ, 995, 26

Hardcastle, M. J., Worrall, D. M., & Birkinshaw, M. 1998, MNRAS, 296, 1098

Heckman, T. M. 1980, A&A, 87, 152

Ho, L. C., Filippenko, A. V., Sargent, W. L. W. 1997, ApJ, 487, 568

Kharb, P., & Shastri, P. 2004, [astro-ph/0401042]

Kormendy, J., & Richstone, D. 1995, ARA&A, 33, 581

Lewis, K. T., Eracleous, M., & Sambruna, R. M. 2003, ApJ, in press [astro-ph/0304399]

Merloni, A., Sebastian, H., & Di Mateo, T. 2003, [astro-ph/0305261]

Morganti, R., Killeen, N. E. B., & Tadhunter, C. N. 1993, MNRAS, 263, 1023

Quataert, E. 2003, Astron. Nachr., 324, 3 [astro-ph/0304099]

Richstone, D., Ajhar, E. A., Bender, R., et al. 1998, Nature, 395, 14

Sadler, E. M., Jenkins, C. R., Kotanyi, C. G. 1989, MNRAS, 240, 591

Sambruna, R. M., Eracleous, M., & Mushotzky, R. 1999, ApJ, 526, 60

Sambruna, R. M., Gliozzi, M., Eracleous, M., Brandt, W. N., & Mushotzky, R. 2003, ApJ, 586,37

Smith, R. K., Brickhouse, N. S., Liedahl, D. A., & Raymond, J. C. 2001, ApJ, 556, L91

Tadhunter, C. N., Morganti, R., Robinson, A., Dickson, R., Villar-Martin, M. & Fosbury, R. A. E. 1998, MNRAS, 298, 1035

Urry, M. C., & Padovani, P. 1995, PASP, 107, 803

Wall, J. V., & Peacock, J. A., 1985, MNRAS, 216, 173

Weingarter, J. C., & Murray, N. 2002, ApJ, 580, 88

Worrall, D. M., & Birkinshaw, M. 1994, ApJ, 427, 134

This preprint was prepared with the AAS LaTeX macros v5.2.

Table 1: Object Sample

Object (1)	Alt. Name (2)	RA (3)	Dec (4)	z (5)	N_H^{Gal} (6)	log M_{BH} (7)	FR (8)	LINER (9)
0034−01	3C 15	00 37 04.1	−01 09 08	0.007	2.9	8.81	I/II	C
0305+03	3C 78	03 08 26.2	+04 06 39	0.029	10.3	8.71	I	PL
0320−37	For A	03 22 41.7	−37 12 30	0.006	1.9	8.31	I	PL
0915−11	Hyd A	09 18 05.7	−12 05 44	0.054	4.9	8.97	I	L
1216+06	3C 270	12 16 23.2	+05 49 31	0.007	1.5	8.72	I	L
1246−41	NGC 4696	12 48 49.3	−41 18 40	0.010	8.1	8.65	I	L
1251−12	3C 278	12 54 36.1	−12 33 48	0.015	3.6	8.64	I	L
1333−33	IC 4296	13 36 39.0	−33 57 57	0.013	4.1	9.16	I/II	L
1637−77	PKS 1637−77	16 44 16.1	−77 15 48	0.043	8.7	8.68	II	L

Note. — **Columns:** (1) object's IAU name; (2) object's common name; (3)-(4) right ascension and declination (Equ J2000) from NED; (5) redshift from NED; (6) Galactic equivalent hydrogen column (in units of 10^{20} cm^{-2}); (7) black hole masses in units of $\log M_{\odot}$ calculated using the velocity dispersion–M_{BH} correlation (Ferrarese 2000), except 0034–01 and 1637–77 from Bettoni et al. 2003, and 1216+06 from Ferrarese et al. 1996; (8) Fanaroff & Riley radio classification from Tadhunter et al. 1998, except for 0034−01 which is from Leahy et al. (1997); (9) classification from Lewis et al. (2003)—L=LINER, PL=Possible LINER, C=Conflicting.

Table 2: Observation Log

Object (1)	Sat (2)	Date (3)	Exp (4)	r_{ext} (5)	Counts (6)
0034−01	CXO	00–11–06	25.4	1.5	493±22
0305+03	SAX	97–01–07	19.4	240	672±27
0320−37	CXO	01–04–17	29.1	1.5	464±22
0915−11	CXO	99–11–02	17.8	1.5	400±20
	XMM	00–12–08	20.2	15.0	28810±170
1216+06	CXO	00–05–06	32.0	1.5	1738±41
	XMM	01–12–16	21.3	20.0	6454±85
1246−41	CXO	00–05–22	31.7	12.0[a]	16719±136
	XMM	02–01–03	40.0	15.0	33055±236
1251−12	CXO	02–06–16	48.6	1.5	154±12
1333−33	CXO	01–12–15	24.3	1.5	1723±42
1637−77	XMM	02–02–23	3.5	15.0	1961±45

Note. — **Columns:** (1) object's name; (2) satellite with which the object was observed—CXO=*Chandra*, XMM=*XMM–Newton*, SAX=*BeppoSAX*; (3) date of observation (yy–mm–dd); (4) effective exposure time in kilo–seconds; (5) radius of circular extraction region centered about the nucleus in arcseconds; (6) background corrected number of counts in the extraction region—the energy range of the counts is depentent upon the detector used: ACIS-S=0.5–8.0 keV, XMM=0.3–10.0 keV, SAX=0.3–10.0 keV.

Table 3: Results of Spatial Analysis

Object	R_c	β	N_β	P_{PSF}
(1)	(2)	(3)	(4)	(5)
0034−01	-	-	-	>99.9
0320−37	4.6±0.3	0.61±0.06	12.59 ± 0.008	>99.9
0915−11	15.9±1.6	0.47±0.10	15.85 ± 0.316	>99.9
1246−41	18.8±2.0	0.64±0.20	12.59 ± 0.199	16.6
1251−12	1.8±0.5	0.49±0.11	2.512 ± 0.631	>99.9
1333−33	0.8_{fixed}	0.56±0.01	199.5 ± 7.943	>99.9

Note. — **Columns:** (1) object's name; (2) core radius in arcseconds; (3) β value; (4) normalization on the β–model in units of 10^{-4}; (5) probability that a PSF is required according to an F–test.

Table 4: Results of Spectral Analysis

Object (1)	model[a] (2)	kT (3)	Abund (4)	N_H^{Add} (5)	CF (6)	EW (7)	Γ (8)	χ^2_{red}/d.o.f. (9)
0034−01	I	-	-	$8.8^{+3.5}_{-2.4}$	0.86±0.06	<170	$1.58^{+0.29}_{-0.32}$	0.73/19
0305+03	IV	-	-	-	-	<1900	$2.74^{+0.26}_{-0.25}$	0.98/31
0320−37	II	0.6±0.1	0.2_{fixed}	$0.3^{+1.3}_{-0.3}$	-	-	$1.78^{+1.21}_{-0.40}$	0.90/15
0915−11	VI	$1.8^{+0.34}_{-0.56}$	$0.2^{+0.05}_{-0.09}$	$6.0^{+6.3}_{-2.4}$	-	<51.3	$2.14^{+1.26}_{-0.58}$	1.03/548
		$4.3^{+2.30}_{-1.01}$	$1.2^{+0.00}_{-0.64}$					
1216+06	III	$0.7^{+0.01}_{-0.02}$	1.0_{fixed}	$5.1^{+1.1}_{-1.2}$	$0.81^{+0.06}_{-0.09}$	230^{+166}_{-134}[c]	$1.46^{+0.17}_{-0.31}$	1.12/359
1246−41	V	0.7±0.01	$1.2^{+0.00}_{-0.07}$	0.1±0.01[b]	-	<374	-	1.23/483
		1.5±0.02	$1.2^{+0.00}_{-0.02}$					
1251−12	VII	0.6±0.1	$1.2^{+0.00}_{-0.93}$	-	-	-	$-0.07^{+0.58}_{-0.69}$	334/435[d]
1333−33	II	0.6±0.3	1.0_{fixed}	$1.1^{+0.6}_{-0.5}$	-	-	$1.52^{+0.42}_{-0.37}$	1.22/66
1637−77	IV	-	-	-	-	<375	1.90±0.06	0.76/88

[a] I=wabs(zpcfabs(powerlaw)); II=wabs(apec+zwabs(powerlaw)); III=wabs(apec+zpcfabs(powerlaw)); IV=wabs(powerlaw); V=wabs(apec+apec); VI=wabs(apec+apec+wabs(powerlaw)); VII=wabs(apec+powerlaw).

[b] This is not an additional absorption component; such a component did not help the fit. This is the number to which the galactic absorption rose when we let it free.

[c] More precise values of E_{line} and σ were able to be fit for this object: $E_{line} = 6.99^{+0.08}_{-0.09}$ keV and $\sigma = 0.03^{+0.15}_{-0.03}$ keV.

[d] Due to the very low number of counts, we used the C–statistics to fit this model. Column (9) therefore gives the C–statistics and the number of pha bins.

Note. — **Columns:** (1) object's name; (2) spectral model (see note); (3) plasma temperature in keV; (4) metal abundances (solar=1.0); (5) Absorption column density at the redshift of the source in units of 10^{22} cm^{-2}; (6) covering fraction; (7) equivalent width in eV at E_{line} = 6.4 keV with the physical width of the Gaussian model fixed at σ = 0.01 keV—see note for 1216+06; (8) photon Index; (9) reduced χ^2 and degrees of freedom.

Table 5: Accretion Properties

Object (1)	L_{bol}/L_{Edd} (2)	$\dot{M}_{Bondi}$ (3)	η (4)
0034−01	6.020	-	-
0305+03	219.5	-	-
0320−37	1.126	0.05	1.106
0915−11	132.2	0.03	1017
0915−11[a]	1234	0.03	9490
1216+06	19.20	0.04	47.28
1246−41	1.825	0.07	2.485
1251−12	0.853	0.05	1.633
1333−33	8.154	6.41	0.407
1637−77	834.3	-	-

[a]Refers to values based on $L_{2-10kev}$ from *XMM–Newton* observation.

Note. — **Columns:** (1) object's name; (2) ratio of the bolometric luminosity to the Eddington luminosity in units of 10^{-6}; (3) Bondi accretion rate in units of $M_\odot$ yr^{-1}; (4) radiative efficiency in units of 10^{-5}.

Table 6: Luminosities

Object (1)	L_{5GHz} (2)	$L_{12_{\mu m}}$ (3)	$L_{[O\ III]}$ (4)	$L_{2-10keV}$ (5)	R (6)
0034−01	41.84		40.41	40.69	−0.64
0305+03	41.84	<45.36	39.12	42.16[a]	−0.44
0320−37	41.24	42.94	<38.65	39.46	−3.40
0915−11	42.58	<46.63	40.27	42.18	−1.80
	-	-	-	43.16[b]	-
1216+06	40.67	42.63	<41.06	40.92[b]	−1.46
1246−41			<38.17	<40.01[b]	
1251−12	40.70	<46.07	<38.70	39.66	−1.44
1333−33	40.99	<44.38	<38.87	41.17	−1.31
1637−77	41.63		40.37	42.70[b]	−1.12

[a]Refers to *BeppoSAX*.

[b]Refers to *XMM–Newton*.

Note. — **Columns:** Values in (2)–(5) are $log(\nu L_\nu)$ (erg s^{-1}). References are as stated below except for 0320–37, 1216+06, and 1333–33 for which the values in columns (2)–(4), (6) come from Sambruna et al. (1999). Column (2) lists the 5 GHz lobe luminosity ($L_{tot}-L_{core}$) from Morganti et al. (1993); column (3) lists the $12_{\mu m}$ luminosity from Golombek et al. (1988); column (4) lists the [O III]λ5007 line luminosity from Tadhunter et al. (1998); column (5) lists the 2–10 keV intrinsic luminosity, where the default intrument is *Chandra*; column (6) lists the R–value from Morganti et al. (1993), defined as the ratio of the core radio luminosity to the lobe radio luminosity at 5 GHz.

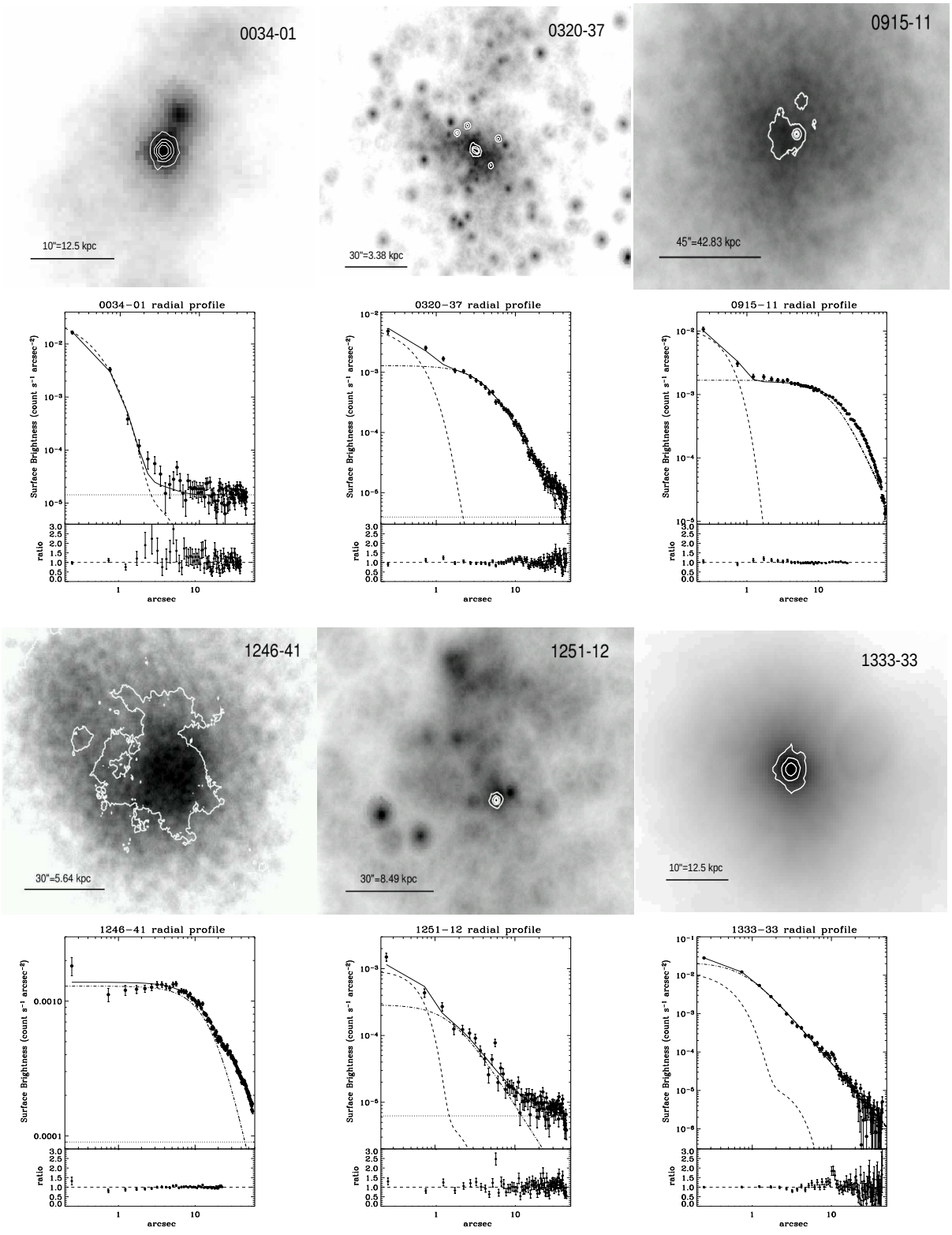


Fig. 1.— Rows 1 and 3 show the adaptively smoothed *Chandra* images in the 0.3–10 keV range, with hard contours (2–10 keV) overlaid. Rows 2 and 4 show the corresponding surface brightness profiles with best–fit (solid line), PSF (dashed line), and β–model (dot–dashed line) overlaid.

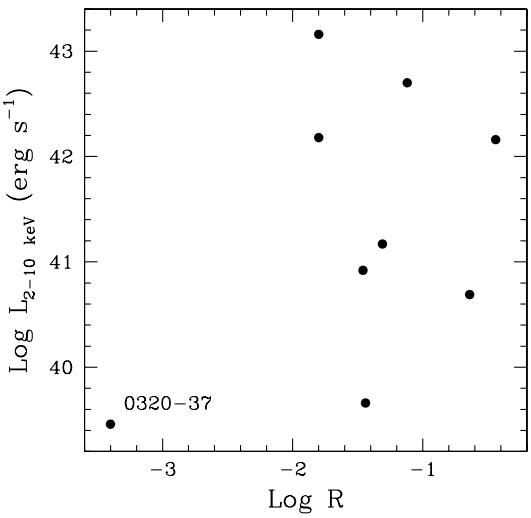


Fig. 2.— Plot of radio core dominance R vs. the 2–10 keV intrinsic luminosity. The parameter R is defined as a ratio of the core-to-lobes 5 GHz luminosities from Morganti et al. (1993). No correlation between the core X–ray luminosity and the radio core dominance is apparent.

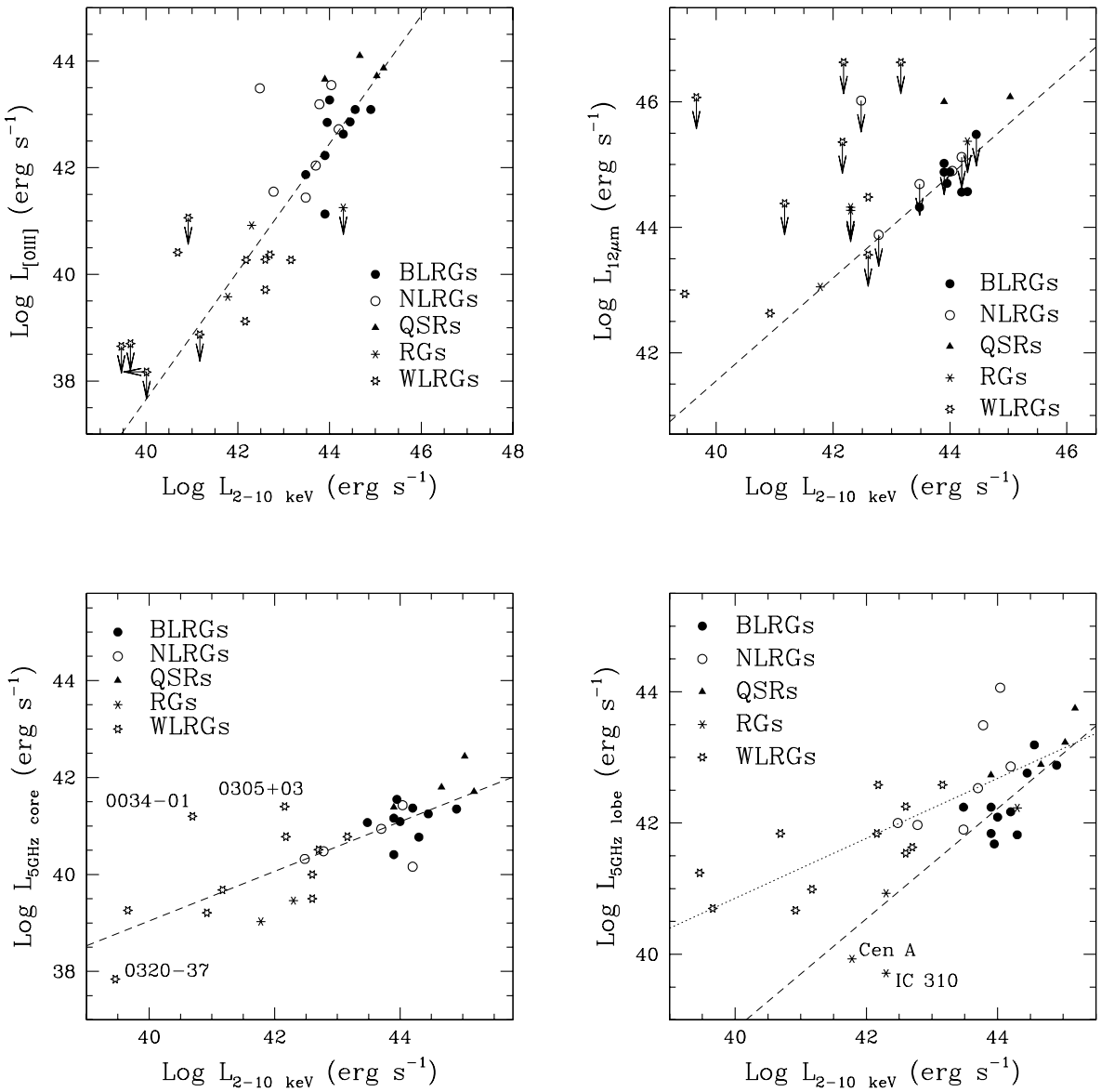


Fig. 3.— The top–left figure shows the correlation between the luminosity of the [O III]λ5007 emission line and the intrinsic 2–10 keV luminosity for various subclasses of radio–loud AGN. Excluding the upper limits, a least squares fit yields the relationship $\log L_{[\mathrm{O_{III}}]} = 1.2\ \log L_{2-10\ \mathrm{keV}} - 10.33$. The top–right figure shows the correlation between the MIR emission at $12\mu m$ and the intrinsic 2–10 keV luminosity. Excluding the upper limits, the correlation is consistent with Sambruna et al. (1999). The bottom–left figure shows the core radio power at 5 GHz and the intrinsic 2–10 keV luminosity; a least squares fit yields the relationship $\log L_{\mathrm{core}} = 0.51\ \log L_{2-10\ \mathrm{keV}} + 18.56$. The bottom–right figure shows the correlation between the lobe radio power at 5 GHz and the intrinsic 2–10 keV luminosity. A least squares fit of the BLRGs, NLRGs, QSRs, and RGs yields the relationship $\log L_{\mathrm{lobe}} = 0.84\ \log L_{2-10\ \mathrm{keV}} + 5.26$ (dashed line). However, the WLRGs formed a distinct group; a least squared fit yields the relationship $\log L_{\mathrm{lobe}} = 0.46\ \log L_{2-10\ \mathrm{keV}} + 22.6$ (dotted line).